

Effective gray scale in lithographically scribed planar holographic Bragg reflectors

Dmitri Iazikov, Christoph Greiner, and Thomas W. Mossberg

We demonstrate that holographic Bragg reflector grating structures, which are photolithographically scribed in planar waveguides, support a unique approach to apodization and overlay that uses fixed-depth etching and partial contour writing to achieve continuous reflective amplitude control. © 2004 Optical Society of America

OCIS codes: 090.2890, 050.1970, 060.2340, 230.7400, 230.1480.

Distributed Bragg reflectors (DBRs) can, in principle, be structured to provide a wide range of spectral filtering functions. In the limit of weak reflectivity, the reflection spectrum of a DBR is simply related to the spatial Fourier transform of its effective reflection coefficient expressed as a function of optical depth into the reflector. Continuous control over the DBR's reflective strength and relative phase as a function of position thus provides the ability to implement arbitrary phase-coherent spectral filtering functions. In the limit of strong reflectivity, the relationship of local reflective amplitude and phase to the spectral transfer function is more complex, but the ability to implement broad ranges of filtering functions remains. Key to the realization of specific filtering functions is the ability to precisely control reflective amplitude and phase as a function of depth within the DBR—even down to the level of individual diffractive elements (lines or planes within the diffractive structure).

Tailoring of DBR spectral filtering functions has been demonstrated in the case of fiber Bragg gratings^{1–7} and channel waveguides^{8–10} by a variety of techniques. Yet none of these methods provides for very high resolution (approaching line-by-line) control of diffractive-element amplitude and phase. Recently a new type of slab-waveguide DBR was pro-

posed¹¹ and demonstrated.¹² These wholly in-plane diffractive structures are called holographic Bragg reflectors (or HBRs) and comprise computer-generated holograms that are lithographically scribed into the core of a two-dimensional (2D) slab waveguide. HBRs are compatible with truly line-by-line amplitude and phase apodization by means that we explore in this paper.

The diffractive elements of an HBR typically consist of lithographically-scribed contours filled with cladding or other dielectric material with a refractive index different from that of the core. HBRs control both the spatial wave front of reflected signals and their spectral content. In principle, HBRs provide a pathway to unique photonic integrated circuits that is based not on constraining wirelike channel waveguides but on integrated, overlapping HBRs that spectrally process and spatially route freely intersecting optical data streams from one active circuit element to another. HBRs provide the power of free-space optics in a fully integrated environment. HBR structures, whose computer-generated diffractive contours provide broad in-plane spatial wave-front transformation capability, contrast with previously discussed lithographically scribed 2D DBRs intended for out-of-plane applications, such as laser feedback and outcoupling^{13–18} and free-space to slab-waveguide beam coupling.^{19–21} Also, the use of holographic imaging made possible with HBRs is generally more powerful than that provided by confocal elliptical DBRs that have been discussed in terms of spectral multiplexing.²²

A simple HBR is schematically shown in Fig. 1. Light enters the slab-waveguide region at the in port and expands within the plane to interact with the multitude of diffractive elements (curved contours). Each diffractive element serves as an imaging device

The authors are with Lightsmyth Technologies, Incorporated, 860 W. Park Street, Suite 250, Eugene, Oregon 97401. T. Mossberg's e-mail address is twmoss@lightsmyth.com.

Received 17 June 2003; revised manuscript received 7 October 2003; accepted 15 October 2003.

0003-6935/04/051149-07\$15.00/0

© 2004 Optical Society of America

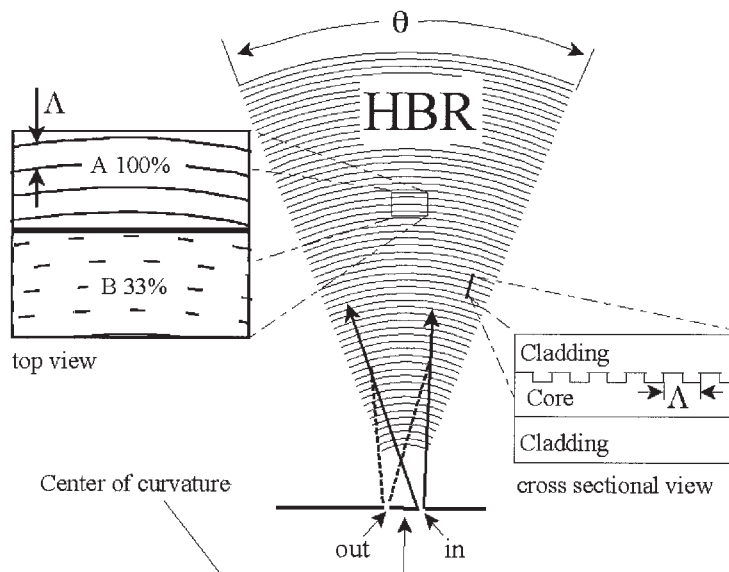


Fig. 1. Schematic of an HBR. Curved contours represent diffractive elements lithographically scribed into the slab waveguide. Each contour backscatters a portion of the entering signal field and focuses it onto the output port. In the devices fabricated for this study, the contours are circular with a common center of curvature shown. The partial-fill effective gray-scale approach to amplitude apodization is shown on the left. The fraction of the contour that is actually populated with an etched trench controls the overall effective amplitude of the field backscattered to the output port by the contour.

that focuses the input signal to the out port. For an HBR operating in the m th order, diffractive elements are spaced by an approximate distance of $\Lambda = m\lambda/2n_{\text{eff}} (m = 1, 2, 3 \dots)$, where λ is the vacuum wavelength of the light to be reflected and n_{eff} is the effective refractive index of the slab waveguide. In Fig. 1 and in the fabricated devices discussed here, the diffractive elements comprise circular cladding-filled trenches that are scribed in the top of the slab-waveguide core layer by means of deep ultraviolet (DUV) photolithography. All diffractive elements share a common center of curvature. As measured along a radius through the center of curvature, the diffractive elements do not have constant spacing. The spacing is set so that signals propagating between the input and the output ports via interaction with the diffractive elements see a constant optical path increment of $m\lambda/2n_{\text{eff}}$ between the diffractive elements.¹¹ This results in a weak chirp in diffractive-element spacing, as measured along a line through the center of curvature. We refer to the line containing the access ports as the input or the output plane as appropriate.

Optimal flexibility in the design of spectral transfer functions requires that there be control over the reflective amplitude and the relative phase of each diffractive element. Relative reflective phase shifts over the range of $\pm\pi$ are provided by spatially displacing diffractive contours over a range $\pm\lambda/4n_{\text{eff}}$. Because HBR contours consist of a computer-generated hologram, which is laser- or electron-beam written onto a standard reticle and then photolithographically scribed onto slab waveguides, full positioning (and hence phase control over the reflective phase) is conveniently available. The reflective am-

plitude of a trenchlike reflective element is determined by various factors, such as trench depth, trench width, and refractive-index contrast between the core and fill materials. Although these factors can, in principle, be used to control the reflective amplitude of the diffractive elements, their practical implementation is inconsistent with convenient lithographic practice, which typically employs a common etch depth across each wafer, uses a single trench-fill material, and is subject to process-related trench-width variations.

However, as we demonstrate here, the 2D nature of HBR devices allows them to be implemented with diffractive elements of variable reflective amplitudes by use of only straightforward lithographic techniques. Referring to Fig. 1 and considering monochromatic input light, one can see that a single diffractive-element contour, k , contributes an amount to the output signal field given by

$$E_{\text{out}}^k \propto \int_{\text{contour } k} E_{\text{in}}(\mathbf{r}) a_k(\mathbf{r}), \quad (1)$$

where $E_{\text{in}}(\mathbf{r})$ and $a_k(\mathbf{r})$ are the input field and the amplitude reflection coefficient, respectively, at contour position \mathbf{r} . It is assumed that the HBR was designed so that contributions to the output field from all locations on the single contour arrive with the same phase, which is necessary for effective imaging. Equation (1) implies that partial contour scribing (i.e., creating a trench along only selected portions of a diffractive-element contour) provides a means of continuously controlling the contour's contribution to the output field without the need for

lithographically challenging variations in diffractive-element trench morphology.

Although the partial scribing approach to achieving continuous reflective amplitude control for individual diffractive elements is conceptually simple, many details must be considered. To preserve the focusing character of the HBR, the partially written diffractive contours must generate substantially the same output wave front as the fully written diffractive-element contour. Either the variation in input field amplitude along the contour must be explicitly considered in determining which portions of a contour to fill, or a fill pattern must be adopted that is immune to a range of input field variations. Furthermore, correlation in the fill pattern between successive diffractive elements must be considered to ensure that portions of the input field do not leak through holes in the HBR structure. Finally, because the effective waveguide refractive index is perturbed, albeit weakly, by the presence of diffractive-element trenches, spatial variations in the effective index that are introduced by partial scribing must be explicitly accounted for in the HBR design process. We refer to the partial writing of diffractive-element contours in HBR devices as “effective gray scale.”

We have fabricated HBR structures to test certain aspects of the effective gray-scale concept. We compare HBRs written with a fixed 0.33 fraction of each contour scribed with HBRs with fully written contours with respect to (1) spatial focusing properties, (2) overall spectral transfer function, and (3) relative reflective strength. The HBRs are designed for reflection at 1.53 μm and are implemented in a silicon-on-silicon format by means of DUV photolithography. Fabricated structures consist of a silicon substrate supporting three silica layers: a lower 15- μm cladding layer, a 6- μm core layer, and an upper 15- μm cladding layer (with a 0.8% core-cladding index contrast). The HBR diffractive elements are scribed at the interface between the core and the upper cladding layers in the form of trenches approximately 250 nm wide and 400 nm deep (see Fig. 1, right). First- and third-order HBRs (with successive diffractive-element contours separated by ~ 0.5 and 1.5 μm , respectively) were fabricated with completely filled (i.e., scribed) diffractive-element contours. Another first-order HBR was partially scribed; that is, only 1/3 of each diffractive contour was etched to produce a trench (see Fig. 1, left). The first-order HBRs have 13,305 diffractive elements. The HBR input and output ports are located symmetrically about the common diffractive-element center of curvature, the structures are 9 mm long from the input-output plane to the final diffractive element and have a 2-mm unscribed free propagation region between the input-output ports and the diffractive elements. Unlike the simple HBR shown in Fig. 1, where diffractive contours subtend a constant angular width, θ , about the center of curvature, diffractive contours of the fabricated HBRs subtend increasingly smaller angles as one moves away from the input-output

plane. Specifically, the diffractive-contour angular width ranges from 0.53 rad at the input-output end to 0.33 rad at the opposite end. The wider opening angle at the input-output end accommodates the 200- μm offset of the input-output ports from the center of curvature. The HBR will provide imaging between any input-output port pair symmetrically located about the center of curvature; however, the weak chirp introduced during the design to equalize contour-to-contour optical path increments will function optimally at the design port separation, which in this case is 400 μm . The measurements presented here utilize the design 400- μm port separation. In the case of the HBR with partially written diffractive-element contours, each contour, k , was divided into 20 equal angular segments of angular width θ_k , with 1/3 of each angular segment lithographically scribed to produce a trench. In box B of Fig. 1 partially written contours are shown with etched trenches (dashes). The dash repetition interval (dash width) subtends an angle θ_k ($\theta_k/3$) relative to the common center of curvature. Owing to the variation in the total angular width subtended by the diffractive contours, θ_k ranges from 0.0165 to 0.0265 rad. The angular segments of successive diffractive elements were given random angular shifts of magnitude $\eta_k\theta_k$, where η_k is a number randomly generated from the interval (0, 1). Some HBRs were fabricated with channel waveguides, and others were constructed without them. In the former case, butt-coupled fibers were connected to channel waveguides, which served as input and output ports precisely positioned at the optimally designed conjugate imaging positions of the HBR. HBRs without channel waveguides were employed to measure output power as a function of position along the output plane.

We first consider the imaging properties of HBRs implemented with effective gray scale (partial contour scribing). The division of each diffractive-element contour into 20 partially scribed segments provides for high-fidelity sampling of the input signal beam. On the other hand, the introduction of a non-continuous, gratinglike structure to the diffractive contour can, in certain cases, introduce ghost structures in the output plane. Theoretical simulation and HBR measurement reveal that, in HBR structures with large numbers of diffractive elements, ghost structures are greatly suppressed by two implemented design factors: the random angular shifts described above and the variation in angular segment size.

In Fig. 2 we show the calculated power as a function of position along the output plane of an HBR with partially scribed diffractive contours and various numbers, N_c , of diffractive contours. Except for Fig. 2(a), which depicts the power distribution produced by a single diffractive contour ($N_c = 1$) of radius 5.5 mm, contours are distributed uniformly throughout the same physical region as the fabricated HBRs. Contour spacing and hence effective diffractive order are adjusted as necessary. Calculations of the output power profile are obtained by

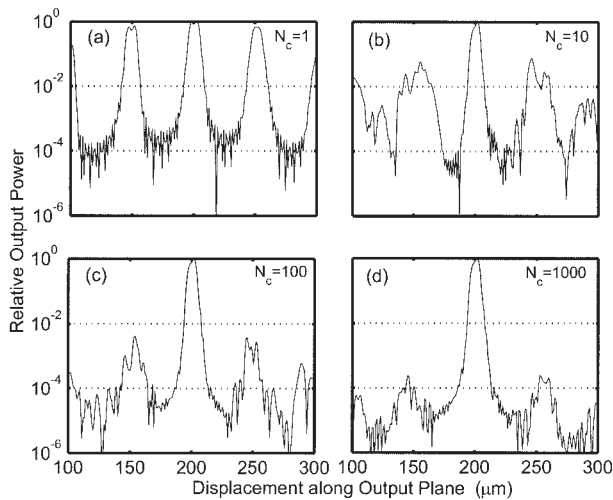


Fig. 2. Simulated output power as a function of position along the output plane for partially written diffractive contours of (a) 1, (b) 10, (c) 100, and (d) 1000, showing the decrease in sidelobe power with increasing contour count. The primary output image is located at 200 μm.

representation of the HBR structures as point scatterers densely spaced along the etched diffractive trenches. The output plane powers shown are derived from an explicit summation of fields diffracted from the input port (10 μm wide with a rectangular field profile), scattered by the representative structure points, and received along the output plane. The input port is positioned at -200 μm, the diffractive-element center of curvature at 0, which places the nominal output port location at +200 μm.

In Fig. 2(a) the power distribution created by a single partially written contour shows a primary image at +200 μm as well as sidelobes of nearly equal strength. The sidelobes correspond to diffractive orders of the segmented contour viewed as a reflective diffraction grating. The sidelobes appear to be equally spaced about the primary image by a distance of $\lambda/\sin \theta_k$, where θ_k is the angular segment width of the single written contour. In Fig. 2(b) an HBR with a total of 10 diffractive contours is analyzed. The sidelobes calculated here are weaker, and they appear to be broadened. The broadening effect arises from the variation in the magnitude of θ_k within the HBR structure. The random angular shift between the scribing patterns of successive diffractive contours has the effect of introducing random phase changes onto the fields contributed by each contour to the sidelobes. These phase changes do not affect the primary image. Owing to the random phase shifts, the sidelobes should decrease in power relative to the primary image by a factor of approximately $1/N_c$ (based on a simplistic random-walk analysis). The variation in θ_k and the random angular shifts together result in an approximately 1.5 order-of-magnitude reduction in sidelobe power relative to the primary image (center peak), even when only 10 contours are written. In Figs. 2(c) and 2(d) the output plane power distribution for $N_c = 100$ and $N_c = 1000$

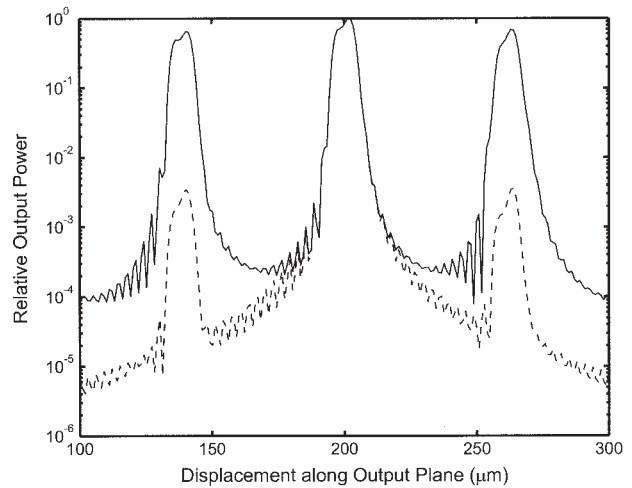


Fig. 3. Simulated output power as a function of position along the output plane for two partially written, 100-contour HBR structures with (dashed curve) and without (solid curve) angular shifts between scribing patterns of successive diffractive contours.

contours, respectively, are displayed. The 1000-contour HBR has a simulated sidelobe reduction of approximately 4 orders of magnitude relative to the primary image. Simulation of the full 13,305-contour fabricated HBR was not performed owing to computational limitations.

In Fig. 3 we display the results of a simulation performed on two partially scribed (0.33 fill-factor) first-order HBR structures, each composed of 100 diffractive contours. All the contours of these structures are located approximately 5.0 mm from the input-output plane and have an identical angular extent. The solid (dashed) curves in Fig. 3 represent the power distribution along the output plane that is produced by an HBR structure whose scribed segments are radially aligned (scribed with random angular shifts as described above). It can be seen that the angular shifting (dashed curve) of the scribed segments strongly suppresses the sidelobe features but does not affect the primary output signal. The exact extent of the sidelobe suppression depends in detail on the distribution of the angular shifts employed. Optimal sidelobe suppression may be obtained by means of deterministic, rather than random, angular shifting of contour scribing patterns.

In Fig. 4 we present simulations of HBRs comprising fully written diffractive contours (no gray scale). The absence of sidelobes in Fig. 4 confirms the introduction of gray-scale partial scribing as the source of the sidelobes observed in Fig. 2.

Measurements of power versus position along the output plane were accomplished by scanning a cleaved single-mode SMF-28 fiber along a line parallel to the planar waveguide edge. The die and fiber were square cut, and the fiber axis was oriented normal to the die edge (i.e., was butt coupled). In Fig. 5(a) we plot output power (solid curve) versus position for a fully written first-order HBR with the input

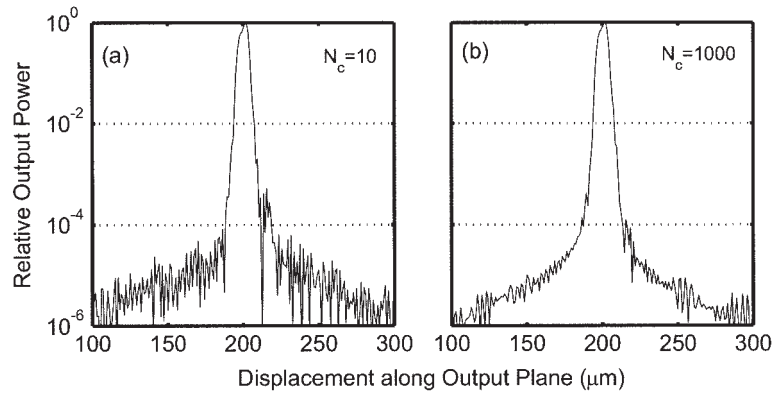


Fig. 4. Simulated output power as a function of position along the output plane for (a) 10 and (b) 1000 fully written continuous diffractive contours. The primary output image is located at 200 μm .

signal wavelength set to maximize HBR reflectivity. The dotted curve at the bottom of the figure represents the scattered light background level as measured with the input laser tuned 20 nm above the HBR resonance wavelength. The focused HBR output is centered at 200 μm , the diffractive-contour center of curvature is located at 0, and the input signal enters at $-200 \mu\text{m}$. The measured output power profile of Fig. 5(a) agrees well with the simulated power profile of Fig. 4(b), considering that the background is not subtracted from the solid curve data of Fig. 5(a). The minimum insertion loss for the measurement of Fig. 5(a) is 3.8 dB, which includes

losses from fiber-to-planar-waveguide coupling. The solid curve of Fig. 5(b) represents measured output power versus output plane position produced by a first-order HBR with each diffractive contour written at the gray-scale level of 0.33. As in Fig. 5(a), the dotted curve in Fig. 5(b) represents off-resonance scattered-light background. Fluctuations in background level with input-signal wavelength and detailed alignment appear to be responsible for the dips in the observed output power below the off-resonance background level. The minimum insertion loss for the data of Fig. 5(b) is 10.8 dB, which again includes coupling loss. In the limit of low reflectivity for both gratings, the peak reflected powers of Figs. 5(b) and 5(a) should be in the ratio of $0.33^2:1$ or -9.6 dB . The measured ratio is larger than this because the fully written first-order grating [Fig. 5(a)] is in the regime of moderately high reflectivity. In Fig. 5(c) we superimpose the output power profiles of the fully (solid curve) and partially written HBRs and normalize them to the same peak value. Presented in this way, the data clearly reveal small sidelobes at approximately 150 and 250 μm on the output plane in the measured output power from the partially written HBR (dotted-dashed curve). The spatial location of the observed sidelobes agrees well with the location expected based on the simulation shown in Fig. 2(d). The observed sidelobe magnitude is somewhat larger than the $\approx 10^{-5}$ expected based on the Fig. 2 simulation when extrapolated to the case of 13,305 diffractive contours. The 40-dB contrast observed between the primary output peak and the gray-scale sidelobe is, however, fully adequate for many applications. It should be noted that the simulated and the fabricated partially written HBRs have not been optimized for sidelobe suppression. The angular pattern shifts and the variation in θ_k may be deterministically controlled during design for more effective sidelobe suppression.

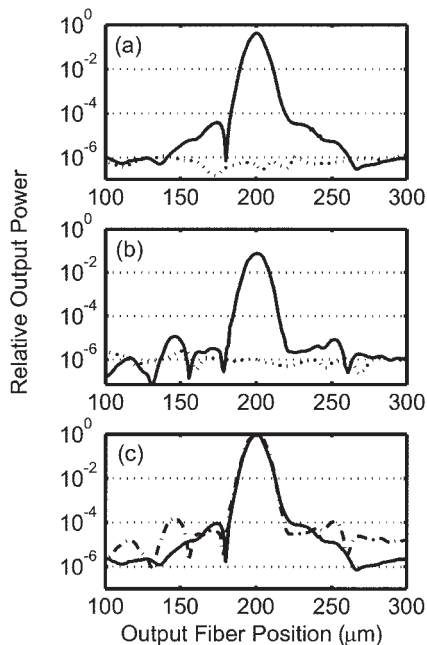


Fig. 5. Measured output power as a function of position along the output plane for (a) fully written first-order HBR, (b) partially written (0.33 fraction) first-order HBR, and (c) superimposed fully and partially written HBR measurements. The lower dotted curve in (a) and (b) represents a background light power level that corresponds primarily to the input signal scattered off the square-die boundaries.

In Fig. 6 we compare spectra and reflected power levels of a first-order, partially written, 0.33-fill-factor HBR (dotted curve) and a third-order, fully written, 1.0-fill-factor HBR (solid curve). The partially written HBR has 33% of each contour written

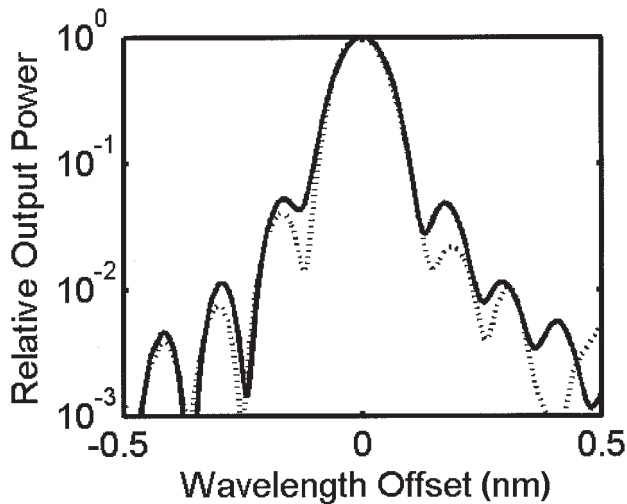


Fig. 6. Superimposed reflection spectra of a 0.33 gray-scale first-order HBR (dotted curve) and a fully written third-order HBR (solid curve). Spectral widths and peak reflectivity are essentially identical, confirming the ability of partial-fill gray scale to control reflection amplitude.

as described above. For the spectral measurement, a die equipped with input and output channel waveguides was employed. Actual spectra are obtained by scanning a fixed polarization test laser across the HBR reflective peak. In Fig. 6 all data are multiplied by a constant factor so that the peak of the solid curve equates to unity. The dashed spectrum is not separately normalized. It is seen that the first-order, 0.33-written HBR and the third-order, 1.0-written HBR have essentially identical reflectivity. This result is fully consistent with our premise that fill factor equates to diffractive amplitude. Applying the gray-scale concept to Fig. 6, we expect that reflected power should scale as the total number of diffractive contours in the HBR multiplied by the fill factor (reflective amplitude) of the contours. Thus we expect the first-order, 0.33-written HBR and the third-order, 1.0-written HBR to have the same reflectivity—as indeed they do.

From Fig. 6 we also see that the reflection spectra of the partially written and the completely written HBRs are virtually identical, as one would expect for first- and third-order HBRs that have the same length and that differ only in the reflective amplitude of their diffractive elements. To facilitate comparison of the spectra, we horizontally shift them to a common wavelength origin. The actual peak reflection wavelengths of the two HBRs are 1530.93 and 1530.75 nm for the first-order, 0.33-filled and third-order, 1.0-filled HBRs, respectively.

In summary, we have studied the use of partial diffractive-element scribing as a means of achieving precise reflective amplitude control in distributed 2D diffractive structures. We find that the spatial imaging and spectral properties of HBR devices are left intact through use of partial contour scribing, provided that simple sidelobe suppression design features are incorporated. We find that, overall,

reflective strength scales as expected with the fraction of diffractive contours scribed with trenches. Demonstrating these performance factors is crucial to the implementation of effective gray-scale methods for general apodization of 2D spectral devices. A remaining factor to be studied is the ability to adjust separations between contours in a heavily apodized structure to compensate for small effective refractive-index changes that are introduced during the process of changing contour fill factors. We point out that partial-fill gray scale can be implemented in slightly modified form in channel-waveguide gratings.²³ We also note that partial-fill gray scale is fully consistent with stamping-based replication of HBR and of other distributed reflector devices.

References

1. T. Erdogan, "Fiber grating spectra," *J. Lightwave Technol.* **15**, 1277–1294 (1997).
2. J. L. Rebola and A. V. T. Cartaxo, "Performance optimization of Gaussian apodized fiber Bragg grating filters in WDM systems," *J. Lightwave Technol.* **8**, 1537–1544 (2002).
3. A. Carballar, M. A. Muriel, and J. Azana, "Fiber grating filter for WDM systems: an improved design," *IEEE Photonics Technol. Lett.* **11**, 694–696 (1999).
4. T. Komukai, K. Tamura, and M. Nakazawa, "An efficient 0.04-nm apodized fiber Bragg grating and its application to narrow-band spectral filtering," *IEEE Photonics Technol. Lett.* **9**, 934–936 (1997).
5. C. Marra, A. Nirmalathas, D. Novak, C. Lim, L. Reekie, J. A. Besley, C. Weeks, and N. Baker, "Wavelength-interleaved OADMs incorporating optimized multiple phase-shifted FBGs for fiber-radio systems," *J. Lightwave Technol.* **21**, 32–39 (2003).
6. K. O. Hill, B. Malo, F. Bilodeau, S. Theriault, D. C. Johnson, and J. Albert, "Variable-spectral-response optical waveguide Bragg grating filters for optical signal processing," *Opt. Lett.* **20**, 1438–1440 (1995).
7. A. Grunnet-Jepsen, A. E. Johnson, E. S. Maniloff, T. W. Mossberg, M. J. Munroe, and J. N. Sweetser, "Fibre Bragg grating based spectral encoder/decoder for lightwave CDMA," *Electron. Lett.* **35**, 1096–1097 (1999).
8. D. Wiesmann, C. David, R. Germann, D. Erni, and G. L. Bona, "Apodized surface-corrugated gratings with varying duty cycles," *IEEE Photonics Technol. Lett.* **12**, 639–641 (2000).
9. D. Wiesmann, R. Germann, G. L. Bona, C. David, D. Erni, and H. Jackel, "Add-drop filter based on apodized surface-corrugated gratings," *J. Opt. Soc. Am. B* **20**, 417–423 (2003).
10. Y. Shibata, T. Tamamura, S. Oku, and Y. Kondo, "Coupling coefficient modulation of waveguide grating using sampled grating," *IEEE Photonics Technol. Lett.* **6**, 1222–1224 (1994).
11. T. W. Mossberg, "Planar holographic optical processing devices," *Opt. Lett.* **26**, 414–416 (2001).
12. C. Greiner, D. Iazikov, and T. W. Mossberg, "Lithographically scribed, focusing, planar holographic Bragg reflector with 17-GHz passband and 0.3 cm² footprint," presented at the Optical Fiber Communication Conference, postdeadline Paper PD31, Atlanta, Ga., March 23–28, 2003.
13. T. Erdogan and D. G. Hall, "Circularly symmetric distributed feedback laser: coupled mode treatment of TE vector fields," *IEEE J. Quantum Electron.* **28**, 612–623 (1992).
14. R. H. Jordan and D. G. Hall, "Highly directional surface emission from concentric-circle gratings on planar optical waveguides: the field expansion method," *J. Opt. Soc. Am. A* **12**, 84–94 (1995).
15. R. H. Jordan, D. G. Hall, O. King, G. Wicks, and S. Rishton,

- “Lasing behavior of circular grating surface emitting semiconductor lasers,” *J. Opt. Soc. Am. B* **14**, 449–453 (1997).
16. A. A. Tovar and G. H. Clark, “Concentric-circle-grating, surface-emitting laser beam propagation in complex optical systems,” *J. Opt. Soc. Am. A* **14**, 3333–3340 (1997).
 17. C. Olson and D. G. Hall, “Azimuthal mode discrimination in radially chirped concentric-circle-grating distributed feedback lasers,” *IEEE J. Quantum Electron.* **36**, 1016–1025 (2000).
 18. S. Kristjansson, N. Eriksson, A. Larsson, R. S. Penner, and M. Fallahi, “Observation of stable cylindrical modes in electrically pumped circular grating-coupled surface-emitting lasers,” *Appl. Opt.* **39**, 1946–1953 (2000).
 19. J. Backlund, J. Bengtsson, C. Carlstrom, and A. Larsson, “In-coupling waveguide holograms for simultaneous focusing into multiple arbitrary positions,” *Appl. Opt.* **38**, 5738–5746 (1999).
 20. M. Li, B. S. Luo, C. P. Grover, Y. Feng, and H. C. Liu, “Waveguide grating coupler with a tailored spectral response based on a computer-generated waveguide hologram,” *Opt. Lett.* **24**, 655–657 (1999).
 21. J. Backlund, J. Bengtsson, C. Carlstrom, and A. Larsson, “Input waveguide grating couplers designed for a desired wavelength and polarization response,” *Appl. Opt.* **41**, 2818–2825 (2002).
 22. C. H. Henry, R. F. Kazarinov, Y. Shani, R. C. Kistler, V. Pol, and K. J. Orlowsky, “Four-channel wavelength division multiplexers and bandpass filters based on elliptical Bragg reflectors,” *J. Lightwave Technol.* **8**, 748–755 (1990).
 23. C. Greiner, T. W. Mossberg, and D. Iazikov, “Bandpass engineering of lithographically scribed channel-waveguide Bragg gratings,” *Opt. Lett.* (to be published).